Thin-layer chromatography

TLC was done on silica gel plates as previously described[17]. Acetyl-CoA and CoA were visualized by UV at 254 nm.

Deacetylation of acetyl-TFIIB

0.1 nmol of [^{14}C]-acetyl-CoA was incubated with 20 pmol rhTFIIB for 40 min, allowing full acetylation. A 50-fold excess of CoA over initial acetyl-CoA was added and the mixture was incubated for the number of hours shown. The results were visualized by SDS–PAGE and autoradiography. The integrity of rhTFIIB after incubation was verified by western blotting with anti-TFIIB antibodies.

Proteolytic determination of acetylation sites

The acetylation site was determined by proteolytic digestion and LC-MS/MS analysis. Protein bands were excised from gels and subjected to limited tryptic digestion, followed by nanoscale reverse-phase HPLC separation of the resulting peptides. Peptides were identified after electrospray ionization into a LCQ DECA ion-trap mass spectrometer. For a peptide coverage of 74% of the protein, K238 is the only acetylated lysine residue.

Site-specific mutagenesis

The construct was mutated using the QuikChange kit (Stratagene) and custom primers (Oligos, Etc.). Mutant constructs were verified by sequencing. Proteins were expressed in *Escherichia coli* and purified as previously described[12]. The presence of TFIIB and its variants was verified by western blot with anti-TFIIB antibodies and a secondary antibody-peroxidase derived coloured reaction.

Immunoaffinity capturing

TFIIB affinity matrices were prepared as previously described[14]. TFIIB and acetyl-TFIIB affinity agarose beads were mixed with highly purified recombinant TFIIB, then with rhTBP or TFIIF (Calbiochem) at ambient temperature. Binding to the TFIIB affinity matrix was monitored by western blotting with mouse monoclonal antibody against TBP (a gift from J. Flint) or rabbit polyclonal antibodies against RAP74 (C-18, Santa Cruz).

In vitro transcription assays

HeLa nuclear extract was depleted of TFIIB using an affinity matrix with covalently attached polyclonal antibody for hTFIIB. Transcription reactions were assembled with depleted nuclear extract, AdMLP G-less supercoiled DNA template[18] and [^{33}P]-UTP. To substitute for endogenous TFIIB different amounts of highly purified rhTFIIB or K238A were added. Activity was then quantified by autoradiography after SDS–PAGE; the 340-nucleotide RNA transcript was generated from AdMLP.

Transfection experiments

Plasmids were purified using a CsCl gradient after Triton X14 treatment and transfected using Fugene 6 (Roche). Cell cultures were treated with lysis buffer 48 h post-transfection, and the luciferase reporter assay system (Promega Corp.) was used with the AdMLP. A β-galactosidase reporter assay system (Tropix) was used with the RSV and SV40 promoters. Cells received 3 μg total plasmid DNA. Co-transfection of 0.5 μg plasmid containing the luciferase gene in the pGL3-45S RNA promoter-EMCV vector (a gift from T. Moss), which does not require TFIIB for transcription, was used as a control to correct for varying transfection efficiencies. Galactosidase data are normalized to the activity seen with the plasmid promoter vector alone ±s.e.m. Transfection experiments were performed in four triplicate sets, with consistent results (s.d. ± 3%).

ChIP assays

The amount of TFIIF and flag-TFIIB variants attached to the co-transfected AdMLP in MBP cells was measured by ChIP assay, using a protocol from Upstate Solutions (with slight modifications). The chromatin was not sonicated. T7 and luciferase primers were used for the PCR amplification of the AdMLP fragment.

Received 12 May; accepted 1 July 2003; doi:10.1038/nature01899.

1. Kouzarides, T. Acetylation: A regulatory modification to rival phosphorylation? *EMBO J.* **19,** 1176–1179 (2000).
2. Orphanides, G., Lagrange, T. & Reinberg, D. The general transcription factors of RNA polymerase II. *Genes Dev.* **10,** 2657–2683 (1996).
3. Bizzozero, O. A., McGarry, J. F. & Lees, M. B. Autoacylation of myelin proteolipid protein with acyl coenzyme A. *J. Biol. Chem.* **262,** 13550–13557 (1987).
4. Yamashita, A., Watanabe, M., Tonegawa, T., Sugiura, T. & Waku, K. Acyl-CoA binding and acylation of UDP-glucuronosyltransferase isoforms of rat liver: Their effect on enzyme activity. *Biochem. J.* **312,** 301–308 (1995).
5. Duncan, J. A. & Gilman, A. G. Autoacylation of G protein alpha subunits. *J. Biol. Chem.* **271,** 23594–23600 (1996).
6. Veit, M. *et al.* Palmitoylation of rhodopsin with *S*-protein acyltransferase: Enzyme catalyzed reaction versus autocatalytic acylation. *Biochim. Biophys. Acta* **1394,** 90–98 (1998).
7. Brownell, J. E. & Allis, C. D. Special HATs for special occasions: Linking histone acetylation to chromatin assembly and gene activation. *Curr. Opin. Genet. Dev.* **6,** 176–184 (1996).
8. Shevchenko, A., Wilm, M., Vorm, O. & Mann, M. Mass spectrometric sequencing of proteins silver-stained polyacrylamide gels. *Anal. Chem.* **68,** 850–858 (1996).
9. Peng, J. & Gygi, S. P. Proteomics: The move to mixtures. *J. Mass Spectrom.* **36,** 1083–1091 (2001).
10. Eng, J., McCormack, A. L. & Yates, J. R. I. An approach to correlate tandem mass spectral data of peptides with amino acid sequences in a protein database. *J. Am. Soc. Mass Spectrom.* **5,** 976–989 (1994).
11. Bagby, S. *et al.* Solution structure of the C-terminal core domain of human TFIIB: Similarity to cyclin A and interaction with TATA-binding protein. *Cell* **82,** 857–867 (1995).
12. Nikolov, D. B. *et al.* Crystal structure of a TFIIB–TBP–TATA-element ternary complex. *Nature* **377,** 119–128 (1995).
13. Yan, Y., Harper, S., Speicher, D. W. & Marmorstein, R. The catalytic mechanism of the ESA1 histone acetyltransferase involves a self-acetylated intermediate. *Nature Struct. Biol.* **9,** 862–869 (2002).
14. Usheva, A. & Shenk, T. YY1 transcriptional initiator: protein interactions and association with a DNA site containing unpaired strands. *Proc. Natl Acad. Sci. USA* **93,** 13571–13576 (1996).
15. Fang, S. M. & Burton, Z. F. RNA polymerase II-associated protein (RAP) 74 binds transcription factor (TF) IIB and blocks TFIIB-RAP30 binding. *J. Biol. Chem.* **271,** 11703–11709 (1996).
16. Luger, K., Rechsteiner, T. J. & Richmond, T. J. Preparation of nucleosome core particle from recombinant histones. *Methods Enzymol.* **304,** 3–19 (1999).
17. Mayer, R. T., Holman, G. M. & Bridges, A. C. Phosphorescence detection method for purine-containing compounds on thin-layer chromatograms. *J. Chromatogr.* **90,** 390–391 (1974).
18. Sawadogo, M. & Roeder, R. G. Factors involved in specific transcription by human RNA polymerase II: Analysis by a rapid and quantitative in vitro assay. *Proc. Natl Acad. Sci. USA* **82,** 4394–4398 (1985).

Supplementary Information accompanies the paper on **www.nature.com/nature**.

Acknowledgements We thank T. Richmond for the gift of recombinant human histone proteins, S. Gygi for proteolytical analysis on acetyl-TFIIB, and S. Robson and M. Gray for critically reading our manuscript. This work was supported by the NIH (A.U.).

Competing interests statement The authors declare that they have no competing financial interests.

Correspondence and requests for materials should be addressed to A.U. (ausheva@caregroup.harvard.edu).

Complex between nidogen and laminin fragments reveals a paradigmatic β-propeller interface

Junichi Takagi[1,3]*, Yuting Yang[2,4]*, Jin-huan Liu[2,4], Jia-huai Wang[2,3] & Timothy A. Springer[1,5]

[1]*The Center for Blood Research, Boston, Massachusetts 02115, USA*
[2]*Dana-Farber Cancer Institute, Boston, Massachusetts 02115, USA*
[3]*Department of Pediatrics,* [4]*Department of Medicine, and* [5]*Department of Pathology, Harvard Medical School, 200 Longwood Avenue, Boston, Massachusetts 02115, USA*

* These authors contributed equally to this work

Basement membranes are fundamental to tissue organization and physiology in all metazoans. The interaction between laminin and nidogen is crucial to the assembly of basement membranes[1–4]. The structure of the interacting domains reveals a six-bladed Tyr-Trp-Thr-Asp (YWTD) β-propeller domain in nidogen bound to laminin epidermal-growth-factor-like (LE) modules III3–5 in laminin (LE3–5). Laminin LE module 4 binds to an amphitheatre-shaped surface on the pseudo-6-fold axis of the β-propeller, and LE module 3 binds over its rim. A Phe residue that shutters the water-filled central aperture of the β-propeller, the rigidity of the amphitheatre, and high shape complementarity enable the construction of an evolutionarily conserved binding surface for LE4 of unprecedentedly high affinity for its small size[5]. Hypermorphic mutations in the Wnt co-receptor LRP5 (refs 6–9) suggest that a similar YWTD β-propeller interface is used to bind ligands that function in developmental pathways. A related interface, but shifted off-centre from the pseudo-6-fold axis and lacking the shutter over the central aperture, is used in the low-density lipoprotein receptor for an intramolecular interaction that is regulated by pH in receptor recycling[10].

The minimal elements of basement membranes seem to be nidogen (entactin), laminin, type IV collagen and perlecan, because they are the only components universally conserved in

Caenorhabditis elegans, *Drosophila* and Chordata[1]. The independent, self-assembling matrices formed by laminins and type IV collagens are linked together by nidogen, which also binds perlecan[2,3]. Nidogen therefore seems to be central in organizing all basal laminae including those in skin, muscle and the nervous system. Laminin and nidogen are secreted by epithelial and mesenchymal cells, respectively[2], and their interaction is important in organogenesis[2–4].

Laminin binding to nidogen has been localized to the third of three globular domains, G3, and its flanking epidermal growth factor (EGF)-6 domain (Fig. 1A)[2,3]. The nidogen G3 domain contains six 45-residue sequence repeats with a YWTD motif that have been predicted to fold into a six-bladed β-propeller domain[11]. The binding site within laminin has been localized to module LE4 in the γ1 subunit[2,12–14].

Co-expression in 293T cells with a LE3–5 fragment of the laminin γ1 subunit enhanced the secretion of His-tagged nidogen-1 G3 fragments, particularly for the shorter G3-II and G3-III fragments (Fig. 1a, b). The YWTD β-propeller domain alone is sufficient to form a stable complex with LE3–5 (Fig. 1b, lane 6). A second nidogen present in vertebrates, nidogen-2 (ref. 3), gave similar results (Fig. 1b, lanes 7 and 8). This redundancy in laminin binding is consistent with the observation that mice deficient in nidogen-1 or nidogen-2 are mildly or not overtly affected[15–17]. The nidogen-1 complex with LE3–5 is stable to purification and storage in physiological buffer. However, the complex dissociates at pH 6 and below (Fig. 1c), in marked contrast to the low-density lipoprotein receptor (LDLR), in which association of the β-propeller domain with LA modules 4 and 5 requires acidic pH (ref. 10).

A crystal structure of the nidogen-1 G3-III complex with laminin LE3–5 was solved by using molecular replacement to a resolution of 2.3 Å (Fig. 2a, Supplementary Table 1). As predicted[11], the nidogen G3 domain assumes a symmetrical six-bladed β-propeller fold. Each β-sheet or 'blade' of the propeller contains four antiparallel β-strands, with β-strand 1 lining the solvent-filled central channel around the pseudo-6-fold symmetry axis, and β-strand 4 outermost and forming the cylindrical side of the propeller (Fig. 2a). The loops are named after the strands they connect; the 4–1 loops and 2–3 loops alternate in anticlockwise order on the 'top' face, whereas the 1–2 and 3–4 loops form the flared 'bottom' face where the central channel is wider. There is an offset of the six YWTD repeats with respect to the blades, so that the three amino-terminal β-strands unite with the carboxy-terminal β-strand to form blade 6, closing the circular topology of the propeller (Fig. 3). Nidogen contains a long-range disulphide bond that connects blade 1 to blade 6 at the bottom of the β-propeller and is unique among YWTD domains (Figs 2a and 3). The long-range disulphide bond is located at a force-bearing point where neighbouring domains connect, and would help to prevent the β-propeller from unravelling when the basement membrane is mechanically stressed.

The structure of LE3–5 bound to nidogen is similar to that of uncomplexed LE3–5 (refs 18, 19), except for a bend in LE3,

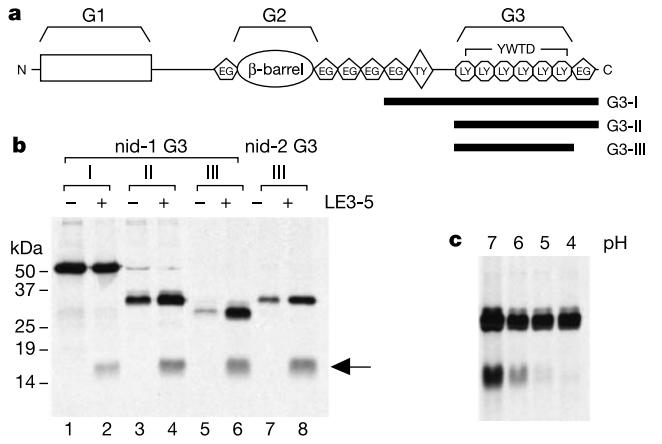

Figure 1 Nidogen and laminin fragment complexes. **a**, Nidogen-1 fragments. EG, EGF module; TY, thyroglobulin repeat; LY, LDL receptor YWTD repeat. **b**, Co-expression of nidogen and laminin γ1 fragments. Material was immunoprecipitated from [^{35}S]methionine and cysteine-labelled culture supernatants with antibody against the V5 tag (Invitrogen) on the nidogen fragment and Protein G–agarose, and subjected to reducing SDS–polyacrylamide-gel electrophoresis. Co-precipitated LE3–5 is marked with an arrow. **c**, Nidogen–laminin association is pH dependent. nidG3-III/LE3–5 immunoprecipitates were incubated at the indicated pH at room temperature for 30 min and washed; material remaining bound was eluted with SDS sample buffer.

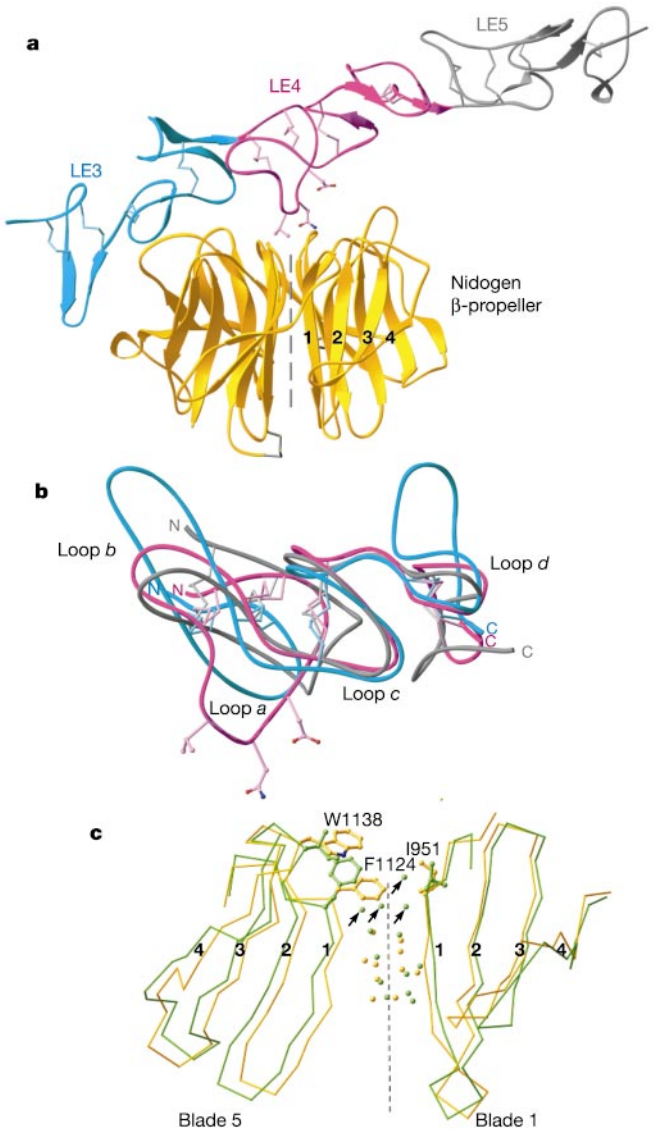

Figure 2 The nidogen β-propeller complex with laminin modules LE3–5 and comparison with the LDLR β-propeller. **a**, Ribbon diagram of the complex. β-strands are numbered on one β-propeller β-sheet. The two disulphide connections are black. **b**, Superposition of LE modules 3 (cyan), 4 (magenta), and 5 (grey). Disulphide connections are thin bonds in the same colour; Asp 800, Asn 802 and Val 804 side chains of LE4 are shown in **a** and **b**. **c**, Superposition of nidogen and LDLR[23] β-propellers showing β-sheets 1 and 5. The Cα trace backbones, side chains and water molecules in the central channel are shown in gold (nidogen) and green (LDLR). Side chains in the hydrophobic shutter in nidogen and equivalent residues in LDLR are shown. The four water molecules present in LDLR and absent in nidogen are marked with arrows. Dashed lines in **a** and **c** represent the pseudo-6-fold axis.

confirming that intermodule interactions give tandem LE modules a rigid rod-like structure (Supplementary Fig. 1A). LE domains are a variant of the EGF fold, with an extra disulphide-bonded *d* loop[20]. The longer disulphide-bonded loops have been designated the *a*, *b*, *c* and *d* loops[18] (Fig. 2b).

LE module 4 docks to an amphitheatre-shaped concave surface centred on the pseudo-6-fold axis atop the β-propeller, whereas LE3 protrudes over the rim of the propeller and exclusively contacts blade 6 (Figs 2a and 3). The unique *a* loop of LE4 (Fig. 2b) forms a prominent, ridge-like protrusion into the amphitheatre of the β-propeller (Fig. 2a). LE3 and LE4 bury similar amounts of total solvent-accessible surface area of 1,000 and 870 Å^2, respectively. However, the shape complementarity[21] of 0.82 at the LE4 interface is much higher, and is also higher than for previously tabulated subunit or receptor–ligand interfaces[21]. In agreement, studies with recombinant LE modules[12] show that the LE4 module makes the predominant contribution to binding affinity, and LE3 is insufficient for binding but augments affinity. LE4 binds with an affinity of $10^9\,M^{-1}$ or more (refs 12–14) yet buries only 870 Å^2, making it the smallest high-affinity interface yet known[5]. The unusual imbalance in burial of 520 Å^2 on LE4 and 350 Å^2 on nidogen reflects the marked convexity and concavity of their binding surfaces, respectively[5].

Rigidity minimizes loss of entropy upon binding and promotes high affinity. On nidogen, rigidity is provided by the concave, amphitheatre-shaped interface (Fig. 4a). The residues in the β-bulge of β-strand 1 (b position; Fig. 3) form the innermost, lower tier of seats in the amphitheatre. Many of these residues point upwards and contact laminin (Figs 3 and 4a), whereas Ile 951 and Phe 1124 point inwards towards the pseudo-symmetry axis and form a hydrophobic shutter that seals off the floor of the amphitheatre (Fig. 4a), shielding it from the water-filled central aperture of the β-propeller that lies just below the binding pocket (Fig. 2c, Supplementary Fig. 1b). The residues immediately preceding β-strand 1 and following β-strand 2, in the 0 position of the β-ladder (Fig. 3), form an outer, higher tier with twice as many seats. These residues point upwards and also form many of the laminin contacts (Fig. 4a). The amphitheatre is strongly rigidified by within-sheet backbone hydrogen bonds, and by between-sheet hydrogen bonds from the side chains of the Thr and Asp of the YWTD motif to backbone. The constraints imposed by packing the bulky side chains that line the amphitheatre onto a concave surface also conspire to create a rigid binding surface.

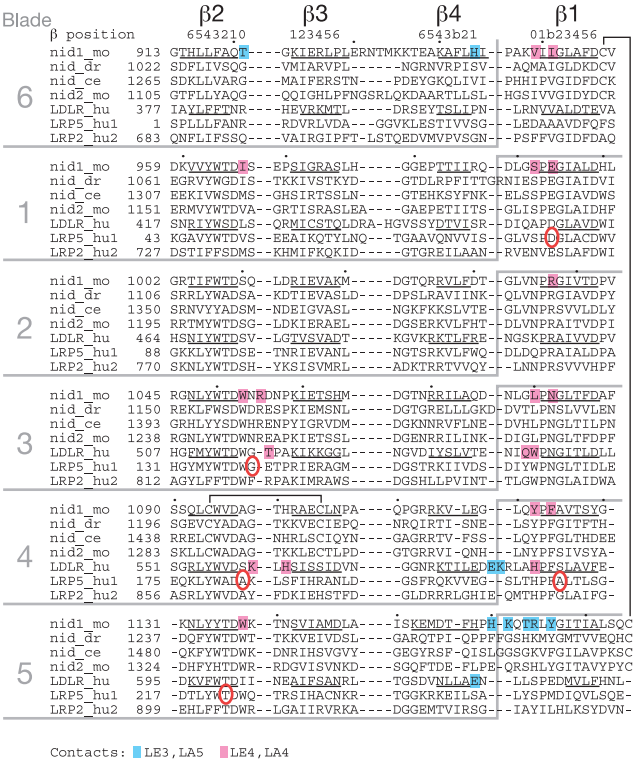

Figure 3 Sequence alignment. Structural alignment of nidogen-1 and LDL receptor[23] β-propeller domains and alignment by sequence to other YWTD domains. mo, mouse; dr, *Drosophila*, ce, *C. elegans*; hu, human; the 1 and 2 suffixes refer to the first and second β-propellers. Each row corresponds to one YWTD repeat; the offset blade boundaries are indicated by grey lines. Blades are structurally aligned, and equivalent β-ladder positions in each strand are numbered at the top of the alignment. β-strands are underlined. Residues in LRP5 known to cause unregulated Wnt signalling in patients with increased bone mass when mutated[6,7,9] are denoted by a red circle; two positions have two independent substitutions each.

The rigidity of the binding surface on laminin is shown by the remarkable similarity of LE4 loop *a* and its side chains in the uncomplexed and complexed LE3–5 structures[18] (Supplementary Fig. 1a). The LE4 loop *a* backbone is well supported by hydrogen bonds (Supplementary Fig. 3), the importance of which is emphasized by the conservation in metazoan evolution of Asp 774 and Asn 806 (Supplementary Fig. 2), which form hydrogen bonds to the loop *a* backbone. Moreover, mutation of loop *c* residues Ile 818 and Tyr 819, which do not interact with nidogen but stabilize loop *a* conformation, reduces the affinity for nidogen by 170-fold and 25-fold, respectively[14].

Interactions within the binding site seem highly efficient. Asn 802 and Val 804 in loop *a* of LE4 protrude most deeply into the propeller amphitheatre, and are centred on the pseudo-6-fold axis (Figs 2a and 4a). The 3,000-fold loss of affinity upon mutation Val 804 → Ser (ref. 14) demonstrates the importance of its hydrophobic interaction with multiple β-propeller amphitheatre residues. The side chain of Asn 802 of LE4 forms two complementary hydrogen bonds to the side chain of Asn 1082 of nidogen (Fig. 4a). The importance of both hydrogen bonds and the stereochemistry of this interaction is demonstrated by the decrease in affinity to 1/5,000 or less after mutation of Asn 802 to Asp, Gln or Ser (ref. 14). Furthermore, the backbone carbonyl of Asn 802 forms bidentate hydrogen bonds to Arg 1037 of nidogen, which also hydrogen bonds with the Asn 802 side chain (Fig. 4a). These interactions are further stabilized by the presence of Arg 1037 at the centre of an extensive network of hydrogen bonds (Supplementary Fig. 3). The side chains of residues Asp 800 of LE4 and Arg 1055 of nidogen form a salt bridge through two charged hydrogen bonds (Fig. 4a). Mutations Asp 800 → Asn and Asp 800 → Glu reduce affinity by 8,000-fold and 70-fold, respectively, confirming the importance of the salt bridge[14]. The importance of residues 800, 802 and 804 agrees with the ability of the *a* loop heptapeptide spanning residues 798–804 to bind to nidogen with an affinity of $10^6\,M^{-1}$ (ref. 13).

In comparison with other extracellular protein recognition interfaces, that between nidogen and laminin module LE4 is unusually conserved. On nidogen, interacting Glu, Asn, Leu, Tyr, two Arg and two Trp residues are invariant in mammalian nidogen-1 and nidogen-2 and in the *C. elegans* and *Drosophila* nidogens, and Val and Ile residues are conserved as aliphatics (Fig. 3). On LE4, Asp 800, Asn 802 and Val 804 are conserved in mammalian γ1 and γ3 laminin subunits, and in the single *Drosophila* and *C. elegans* γ subunits, with the exception of a conservative Val → Ile substitution in *C. elegans* (Supplementary Fig. 2). Notably, *Drosophila* laminin binds to mammalian nidogen[22]. The extreme conservation of the nidogen-LE4 interface suggests that it is highly optimized structurally.

In contrast to nidogen, all other proteins that contain YWTD β-propeller domains are cell surface receptors[11]. Many function as endocytic receptors, such as the LDLR[11,23], and many also function in developmental pathways, including photoreceptor cell development in *Drosophila*, head regeneration in *Hydra*, and neuronal positioning and bone development in vertebrates[24,25]. The recent

structure of the extracellular fragment of the LDLR at endosomal pH shows that the lipoprotein-binding LDLR type A (LA) modules 4 and 5 loop back and bind to the YWTD β-propeller domain, suggesting a function in receptor recycling[10]. Histidines have central positions in the intramolecular LDLR interface but not in the nidogen–laminin interface, which is consistent with the distinct pH preferences of these interactions. The LA4 and LA5 modules of the LDLR also bind lipoprotein ligands, in agreement with a role of the β-propeller domain in ligand release and receptor recycling at endosomal pH. LA4 binds to the top face of the β-propeller using evolutionarily conserved residues[10], similar to the interaction of LE4 with nidogen. However, in contrast to LE4, LA4 has no loop that inserts into the hub of the β-propeller (Fig. 4b), and LA4 binds off-centre (Fig. 4c). Whereas LE4 contacts all six blades of the nidogen β-propeller, LA4 contacts only blades 3, 4 and 5 (Figs 3 and 4c). Like LA5, LE3 binds over the rim of the β-propeller (Fig. 4b, c). The highest projection from the rim is formed by the 2–3 loop of blade 3, which interacts with both LE4 and LA4 (Fig. 3), whereas the shortest 2–3 loop is in blade 6, near the LE3 and LA5 interaction sites. This asymmetric length of loops on opposite sides of the β-propeller rim is

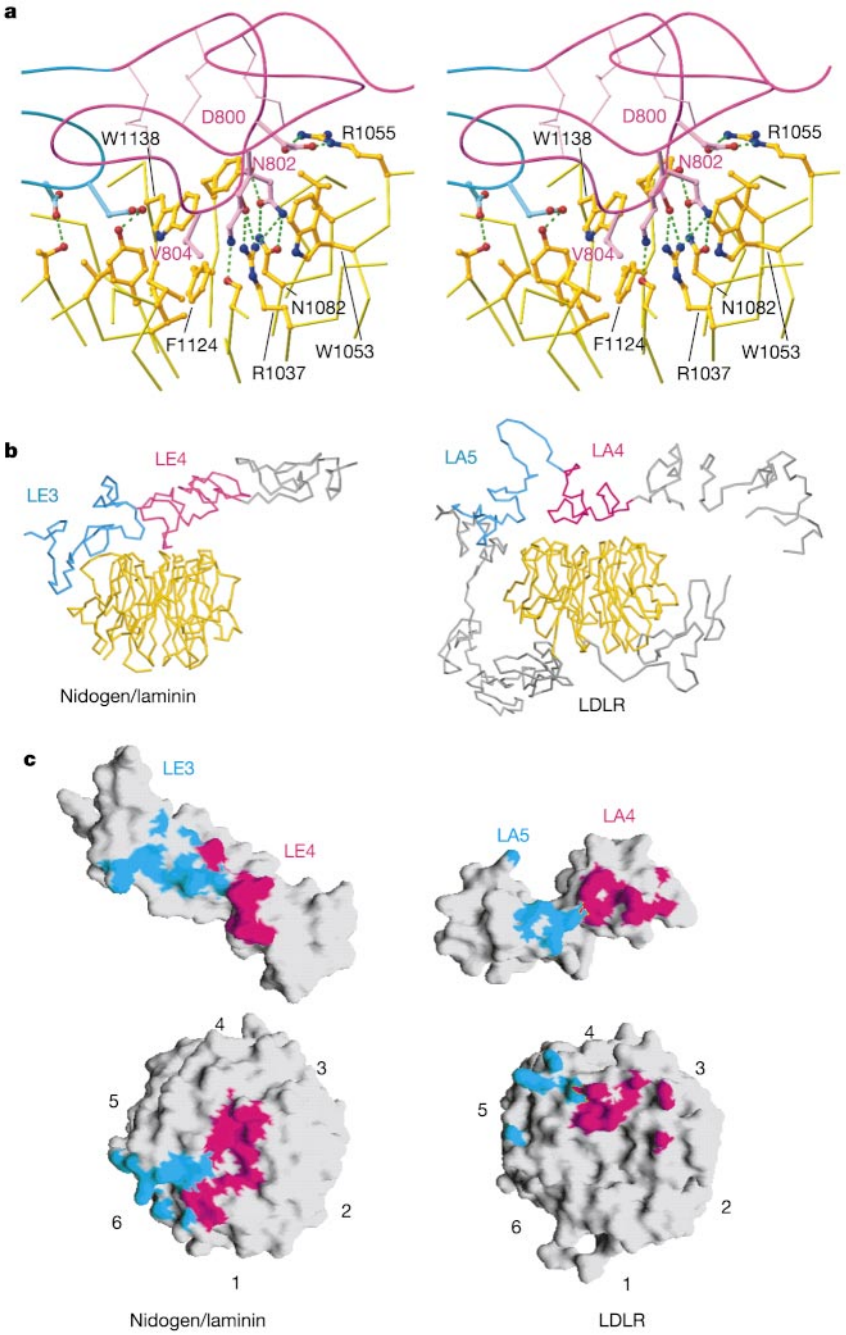

Figure 4 The nidogen–laminin interaction and comparison with the interaction in the LDLR. **a**, Stereo view of the nidogen interaction with LE4 and the adjacent portion of LE3. LE3 and LE4 are as in Fig. 2a. Portions of the nidogen backbone as Cα-trace and side chains forming the amphitheatre are shown in gold. Green dashed lines represent hydrogen bonds. **b**, Cα trace representation of the nidogen–laminin and intrinsic LDLR interactions. The propeller axes are vertical in the page. For clarity, the views are towards β-propeller blade 1 in nidogen and blade 6 in LDLR. **c**, GRASP surfaces. Atoms within 4 Å of an interaction partner are shown in magenta (LE4 and LA4) and cyan (LE3 and LA5). The β-propeller domains are viewed down their 6-fold axes. In the open book representation, the interacting LE3–4 or LA4–5 module pairs are rotated through 180° in the horizontal plane of the page. β-propeller blades are numbered.

characteristic of YWTD β-propellers (Fig. 3), and correlates with the slanted orientation with which both the LE and LA modules bind (Fig. 4b).

Remarkably, the LDLR YWTD β-propeller domain differs from that of nidogen in lacking closure of the bottom of the binding pocket in the hub of the β-propeller. The 1.5-Å crystal structure of the LDLR β-propeller module[23] reveals a continuous column of water that extends all the way through the central cavity (Fig. 2c). In nidogen, Phe 1124 in β-strand 1 of blade 5 acts as a shutter to close the central aperture, whereas the equivalent Phe residue in the LDLR points upward and does not block the aperture (Fig. 2c, Supplementary Fig. 1b). The key difference is that in the upper, outer tier of residues in blade 5, Trp 1138 in the 2–3 loop of nidogen substitutes for an Ile in the LDLR (Fig. 3). The bulky Trp 1138 in nidogen pushes Phe 1124 into the central aperture, ensuring the hydrophobicity of the LE4-binding pocket (Fig. 2c). Furthermore, in the nidogen β-propeller, blades 1 and 5 are closer to the pseudo-6-fold axis by 0.8 and 1 Å, respectively than in either LDLR structure[10,23] (Fig. 2c). Together with the Phe 1124 shutter, this closer packing excludes four water molecules from the nidogen β-propeller that are present at the narrow, upper portion of the central channel in the LDLR, and ensure a hydrophobic binding pocket with a low dielectric constant. The hydrophobic shutter in nidogen seems important for its high affinity for laminin. Because in the LDLR the LA4 and LA5 modules are covalently tethered to the β-propeller domain, high affinity is not required for their interaction.

The concept that YWTD β-propeller domains can bind extrinsic ligands with high affinity, and can also bind intrinsic ligands and promote receptor recycling after endocytosis, has important implications for the increasingly large family of receptors that contain YWTD domains and function in regulating development as well as in endocytosis[24,25]. Many ligands may bind to YWTD domains rather than LA modules, and binding to YWTD domains might affect signalling directly, enable binding to co-receptors, antagonize binding to intrinsic LA module ligands, or affect receptor endocytosis and recycling. Of particular relevance are LRP5, LRP6 and *Drosophila* Arrow, each of which has four YWTD domains, acts as a Wnt co-receptor and also binds with nanomolar affinity to cysteine-rich domains in Dickkopf proteins. Mutations in LRP5 that eliminate its expression lead to reduced bone mass in humans[8]. By contrast, a mutant LRP5 that causes high bone mass[6,9] remains activatable by Wnt but not its antagonist Dickkopf-1 (ref. 9). Remarkably, of seven independent hypermorphic amino acid substitutions in LRP5, all map to the first YWTD β-propeller domain, in positions that are structurally equivalent to the binding site in nidogen for LE4 (Fig. 3). The mutations in YWTD β-propeller 1 of LRP5 all lie in the 4–1 and 2–3 loops of blades 2, 3, 4 and 5. In the number of blades included, the participation of residues that are deep in the central amphitheatre such as Asp 80 (Fig. 3), the predicted presence of a Phe shutter, and high affinity for ligand, the binding modality of LRP5 more resembles that of nidogen than the LDLR β-propeller domain. These results suggest that the high-affinity ligand-binding site described here may be paradigmatic for signalling receptors that bear YWTD domains, as well as of importance in the formation of basement membranes. □

Methods

Expression constructs for nidogen (entactin) fragments contained the authentic signal sequence and various segments from the G3 domain, followed by C-terminal V5 epitope and hexahistidine tags. Nidogen-1 fragments were G3-I, mature amino acid residues 774–1217; G3-II, 913–1217; and G3-III, 913–1179. The nidogen-2 G3-III fragment contained residues 1105–1373. Mouse entactin complementary DNA (a gift from A. E. Chung) or mouse entactin-2 cDNA (a gift from M. Shimane)[3] were used as PCR templates. The mouse laminin γ1 chain encompassing LE3–5 (residues 736–899) was amplified from mouse spleen cDNA library and cloned downstream of a signal sequence without any tag. Complex between nidG3-III and LE3–5 was transiently expressed in 293-EBNA human kidney cells in serum-free medium using episomal expression vectors pCEP4 (Invitrogen) and pCEP-Pu (a gift from R. Timpl)[26] and purified from culture supernatant by Ni-affinity chromatography after dialysis against 25 mM Tris-HCl pH 8.0, 150 mM NaCl, and eluted with 250 mM imidazole in the same buffer. The complex (~7 mg) was treated with 10 μg ml^{-1} chymotrypsin at room temperature for 2 h to remove the flexible tag segment, further purified by Mono Q chromatography (50 mM Tris-HCl pH 8.5, eluted with a NaCl gradient), dialysed against 10 mM Tris-HCl pH 7.5 containing 10 mM NaCl, and concentrated.

Crystals were grown in hanging drops at room temperature by mixing equal volumes of protein (13 mg ml^{-1}) and reservoir solution (1 M sodium acetate, 0.05 M $CdSO_4$, 0.1 M HEPES pH 7.5). The crystal was transferred to reservoir solution supplemented with 20% (v/v) glycerol and flash-frozen in liquid nitrogen.

Data were collected on beamline 19-ID at the Advanced Photon Source at Argonne National Laboratory (Argonne, Illinois), and processed with program HKL2000 (ref. 27). The structure was solved with molecular replacement using program AmoRe[28] with a two-body search in the 15–3.5-Å range with models of the LDLR YWTD domain[23] and LE3–5 (ref. 18). The rotation function peaks for LE3–5 stood out significantly, and the correct one for nidogen was the third highest. A significant translation function was first found for LE3–5, and with LE3–5 fixed, a highly significant translation function was found for nidogen. There is one complex per asymmetric unit. Rigid body refinement yielded a clean map in which main-chain and side-chain density was easily seen for model rebuilding with O. The model was refined to 2.3 Å resolution using simulated annealing in CNS version 1.1 (ref. 29). Six Cd^{2+} ions are bound to the complex. Two interact with the β-propeller only. Four are at boundaries between nidogen and LE3–5 and to some extent are involved in crystal packing, but do not have a specific role in complex formation, as confirmed by lack of effect of EDTA on complex stability (data not shown).

For β-propeller blade superpositions, blades from nidogen and LDLR[23] were cut out and all 12 were simultaneously structurally aligned using 3DMALIGN of Modeller 6.0 (ref. 30). For β-propeller superpositions, all equivalent residues determined by blade superposition were used.

Received 10 March; accepted 26 June 2003; doi:10.1038/nature01873.

1. Hynes, R. O. & Zhao, Q. The evolution of cell adhesion. *J. Cell Biol.* **150,** F89–F96 (2000).
2. Mayer, U., Kohfeldt, E. & Timpl, R. Structural and genetic analysis of laminin–nidogen interaction. *Ann. N.Y. Acad. Sci.* **857,** 130–142 (1998).
3. Timpl, R. in *Guidebook to the Extracellular Matrix, Anchor, and Adhesion Proteins* (eds Kreis, T. & Vale, R. D.) 455–457 (Oxford Univ. Press, 1999).
4. Willem, M. *et al.* Specific ablation of the nidogen-binding site in the laminin γ1 chain interferes with kidney and lung development. *Development* **129,** 2711–2722 (2002).
5. Lo Conte, L., Chothia, C. & Janin, J. The atomic structure of protein–protein recognition sites. *J. Mol. Biol.* **285,** 2177–2198 (1999).
6. Little, R. D. *et al.* A mutation in the LDL receptor-related protein 5 gene results in the autosomal dominant high-bone-mass trait. *Am. J. Hum. Genet.* **70,** 11–19 (2002).
7. Van Wesenbeeck, L. *et al.* Six novel missense mutations in the LDL receptor-related protein 5 (LRP5) gene in different conditions with an increased bone density. *Am. J. Hum. Genet.* **72,** 763–771 (2003).
8. Gong, Y. *et al.* LDL receptor-related protein 5 (LRP5) affects bone accrual and eye development. *Cell* **107,** 513–523 (2001).
9. Boyden, L. M. *et al.* High bone density due to a mutation in LDL-receptor-related protein 5. *N. Engl. J. Med.* **346,** 1513–1521 (2002).
10. Rudenko, G. *et al.* Structure of the LDL receptor extracellular domain at endosomal pH. *Science* **298,** 2353–2358 (2002).
11. Springer, T. A. An extracellular β-propeller module predicted in lipoprotein and scavenger receptors, tyrosine kinases, epidermal growth factor precursor, and extracellular matrix components. *J. Mol. Biol.* **283,** 837–862 (1998).
12. Mayer, U. *et al.* A single EGF-like motif of laminin is responsible for high affinity nidogen binding. *EMBO J.* **12,** 1879–1885 (1993).
13. Poschl, E., Fox, J. W., Block, D., Mayer, U. & Timpl, R. Two non-contiguous regions contribute to nidogen binding to a single EGF-like motif of the laminin gamma 1 chain. *EMBO J.* **13,** 3741–3747 (1994).
14. Poschl, E. *et al.* Site-directed mutagenesis and structural interpretation of the nidogen binding site of the laminin γ1 chain. *EMBO J.* **15,** 5154–5159 (1996).
15. Murshed, M. *et al.* The absence of nidogen 1 does not affect murine basement membrane formation. *Mol. Cell. Biol.* **20,** 7007–7012 (2000).
16. Dong, L. *et al.* Neurologic defects and selective disruption of basement membranes in mice lacking entactin-1/nidogen-1. *Lab. Invest.* **82,** 1617–1630 (2002).
17. Schymeinsky, J. *et al.* Gene structure and functional analysis of the mouse nidogen-2 gene: Nidogen-2 is not essential for basement membrane formation in mice. *Mol. Cell. Biol.* **22,** 6820–6830 (2002).
18. Stetefeld, J., Mayer, U., Timpl, R. & Huber, R. Crystal structure of three consecutive laminin-type epidermal growth factor-like (LE) modules of laminin γ1 chain harboring the nidogen binding site. *J. Mol. Biol.* **257,** 644–657 (1996).
19. Baumgartner, R. *et al.* Structure of the nidogen binding LE module of the laminin γ1 chain in solution. *J. Mol. Biol.* **257,** 658–668 (1996).
20. Bork, P., Downing, A. K., Kieffer, B. & Campbell, I. D. Structure and distribution of modules in extracellular proteins. *Q. Rev. Biophys.* **29,** 119–167 (1996).
21. Lawrence, M. C. & Colman, P. M. Shape complementarity at protein/protein interfaces. *J. Mol. Biol.* **234,** 946–950 (1993).
22. Mayer, U., Mann, K., Fessler, L. I., Fessler, J. H. & Timpl, R. Drosophila laminin binds to mammalian nidogen and to heparan sulfate proteoglycan. *Eur. J. Biochem.* **245,** 745–750 (1997).
23. Jeon, H. *et al.* Implications for familial hypercholesterolemia from structure of the LDL receptor YWTD-EGF domain pair. *Nature Struct. Biol.* **8,** 499–504 (2001).
24. Herz, J. & Bock, H. H. Lipoprotein receptors in the nervous system. *Annu. Rev. Biochem.* **71,** 405–434 (2002).
25. Strickland, D. K., Gonias, S. L. & Argraves, W. S. Diverse roles for the LDL receptor family. *Trends Endocrinol. Metab.* **13,** 66–74 (2002).

26. Kohfeldt, E., Maurer, P., Vannahme, C. & Timpl, R. Properties of the extracellular calcium binding module of the proteoglycan testican. *FEBS Lett.* **414,** 557–561 (1997).
27. Otwinowski, Z. & Minor, W. Processing of X-ray diffraction data collected in oscillation mode. *Methods Enzymol.* **276,** 307–326 (1997).
28. Navaza, J. Amore: An automated package for molecular replacement. *Acta Crystallogr. A* **50,** 157–163 (1994).
29. Brunger, A. T. *et al.* Crystallography & NMR System: a new software suite for macromolecular structure determination. *Acta Crystallogr. D* **54,** 905–921 (1998).
30. Sali, A. & Blundell, T. L. Comparative protein modelling by satisfaction of spatial restraints. *J. Mol. Biol.* **234,** 779–815 (1993).

Supplementary Information accompanies the paper on **www.nature.com/nature**.

Acknowledgements We thank R. Zhang and A. Joachimiak for beamline help, and S. Blacklow and R. Timpl for critically reading the manuscript. This work was supported by an NIH grant.

Competing interests statement The authors declare that they have no competing financial interests.

Correspondence and requests for materials should be addressed to T.A.S. (springeroffice@cbr.med.harvard.edu) or J.W. (jwang@red.dfci.harvard.edu). The PDB code for the nidogen/laminin complex is 1NPE.

corrigendum

^{146}Sm-^{142}Nd evidence from Isua metamorphosed sediments for early differentiation of the Earth's mantle

Guillaume Caro, Bernard Bourdon, Jean-Louis Birck & Stephen Moorbath

Nature **423,** 428–432 (2003).

In this Letter, the subscripts l and k were accidentally transposed, so coefficient A in equation (4) should have read:

$$A = \frac{\ln(m_i/m_j)\ \ln(m_i/m_l)}{\ln(m_k/m_j)\ \ln(m_k/m_l)}$$ □

errata

Links between signal transduction, transcription and adhesion in epithelial bud development

Colin Jamora, Ramanuj DasGupta, Pawel Kocieniewski & Elaine Fuchs

Nature **422,** 317–322 (2003).

In Figs 1e and 2j, k of this paper, the colour keys are incorrect. In Fig. 1e, the blue bars indicate TOPFLASH and the purple bars indicate FOPFLASH. The description of the results in the text is correct. In Fig. 2j and k, the green fluorescence indicates P-cadherin (Pcad) and E-cadherin (Ecad), respectively, and the red fluorescence indicates the marker for the basement membrane, laminin (lam). □

Class 3 semaphorins control vascular morphogenesis by inhibiting integrin function

Guido Serini, Donatella Valdembri, Sara Zanivan, Giulia Morterra, Constanze Burkhardt, Francesca Caccavari, Luca Zammataro, Luca Primo, Luca Tamagnone, Malcolm Logan, Marc Tessier-Lavigne, Masahiko Taniguchi, Andreas W. Püschel & Federico Bussolino

Nature **424,** 391–397 (2003).

In Figs 3c, g and 4c, g of this Article, the colour keys are incorrect. The light grey and white boxes were interchanged. The description of the results in the text is correct. □

